photonics

MDPI

Article

High Electric Field Enhancement Induced by Modal Coupling for a Plasmonic Dimer Array on a Metallic Film

Jiawei Liu [1], Ziming Meng [1,2,*] and Jinyun Zhou [1,2,*]

[1] School of Physics and Optoelectronic Engineering, Guangdong University of Technology, Guangzhou 510006, China
[2] Guangdong Provincial Key Laboratory of Information Photonics Technology, Guangdong University of Technology, Guangzhou 510006, China
* Correspondence: mengzm@gdut.edu.cn (Z.M.); zhjy@gdut.edu.cn (J.Z.)

Abstract: A giant electric field on a subwavelength scale is highly beneficial for boosting the light–matter interaction. In this paper, we investigated a hybrid structure consisting of a hemispheric dimer array and a gold film and realized resonant mode coupling of the surface lattice resonance (SLR) and surface plasmon polariton (SPP). Mode coupling is demonstrated by observing anti-crossing in reflection spectra, which corresponds to Rabi splitting. Although the resonance coupling does not enter the strong coupling regime, an improved quality factor (Q~350) and stronger electric field enhancement in the gap region of the dimer (i.e., hot spot) in our hybrid structure are obtained compared to those of the single dimer or dimer array only. Remarkably, the magnitude of electric field enhancement over 500 can be accessible. Such high field enhancement makes our hybridized structure a versatile platform for the realization of ultra-sensitive biosensing, low-threshold nanolasing, low-power nonlinear optical devices, etc.

Keywords: field enhancement; nanoparticle dimmer; mode coupling; surface plasmon polariton; surface lattice resonance

Citation: Liu, J.; Meng, Z.; Zhou, J. High Electric Field Enhancement Induced by Modal Coupling for a Plasmonic Dimer Array on a Metallic Film. *Photonics* **2024**, *11*, 183. https://doi.org/10.3390/photonics11020183

Received: 15 January 2024
Revised: 13 February 2024
Accepted: 13 February 2024
Published: 17 February 2024

1. Introduction

Plasmonics is a field that has emerged in recent years at the intersection of photonics, electronics, and nanotechnology [1,2] So far, there have been tremendous advances and new developments in plasmonics, as well as in nanophotonics and metamaterials [3]. Plasmonics uses the collective motion of conduction electrons in metals to enable the coupling of light to nanomaterials and to produce a range of optical effects on the nanoscale [4]. At the same time, the collective oscillation of the electrons leads to a localization of the field and its significant enhancement with respect to the excitation field [5]. Two of these properties, localization and enhancement, are among the main components of light that allow guiding and manipulating the diffraction limit [6]. Field localization and enhancement are central in applications such as surface-enhanced Raman spectroscopy (SERS) [7], single-molecule detection [8], high sensitivity photoelectric detection [9], photocatalysts [10], biomedicine [11,12], near-field optical capture [13], and nanoscale light sources [14].

One of the main powerful methods used in sensors is surface-enhanced Raman spectroscopy (SERS), which is the enhancement of the Raman signal achieved by placing Raman-active molecules in the vicinity of the near field of a metallic nanostructure [15]. When two nanoparticles are in close proximity to form a cell, a strong field enhancement and localization within a few cubic nano meters of space between the two nanoparticles is created, which is called a hot spot [16]. Since the Raman signal is proportional to the fourth power of the electric field, high field enhancement between dimer gaps can enhance the Raman signal very well, and the field enhancement of small gaps can locate small molecules between them very well. Nano-cubes, nanospheres, nanorods, and nano-bowtie dimers

are currently being studied [17–20]. How to obtain greater field enhancement between the dimer gaps is what needs to be investigated at present.

Further ways to enhance the field strength between nanodimers are coupling effects or the formation of Fabry–Perot (FP) thin film cavities, such as coupling between surface lattice resonance (SLR) and surface plasmon polariton (SPP) and the formation of FP cavity between arrays and gold films; in addition, the bound states in the continuum (BIC) also proposes an effective method for achieving high Q resonance, and at the same time, giant electric field enhancement simultaneously occurs in quasi-BICs [21,22]. Quite recently, research was conducted on the structure composed of gold nanoparticle arrays and metallic films, and it was found that there is a perfect absorption pair related to phase singularities [23]. However, the explicit field enhancement effect in the systems of metallic nanoparticle arrays and metallic films is still rarely reported. In this study, we investigate structures consisting of metallic dimer arrays and metallic films. The array and the film form an FP cavity, and the 2D array can excite the SLR and the SPP on the gold film. When the gap between the array and the gold film is in a certain range, the SLR and the SPP are coupled. Within this range, this structure can effectively reduce the plasmon linewidth and produce a large near-field enhancement in the gap of a gold plasmonic hemispherical dimer. The near-field enhancement of our dimer array coupled with the metal film structure is about twice as large as that of the dimer array structure alone and has seven times the quality factor increase compared with the SLR. Finally, our simulation results can be verified by using a coupled oscillator model.

2. Simulations and Methods

Figure 1 shows a perspective view of the metal film and dimer array system studied in this paper, which consists of a gold film and a periodic hemispheric dimer array placed on the gold film. The thickness of the gold film is set to 200 nm, preventing any light transmission. The dimer consists of two hemispheres with a radius of 75 nm and the gap g between the two hemispheres is set to 6 nm. The dimer array is periodically arranged in the x-y plane with the period in the x-direction P_x = 800 nm and the period in the y-direction P_y = 800 nm, initially. The dielectric properties of the array and the gold films were taken from the CRC database in the software ANSYS Lumerical [24]. The incident light source is linearly polarized along the x-direction and impinges the structure vertically along the z-direction. For simplicity without loss of generality, the ambient refractive index of the structure was set to 1.0. The finite-difference time-domain (FDTD) method is used to investigate the optical response of our hybrid structures.

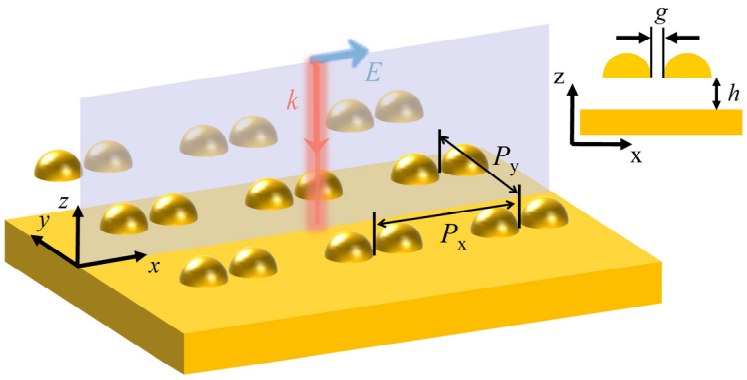

Figure 1. Schematic illustration of the hybrid structure composed of a gold hemispherical dimers array on a thick gold film. The inset is the cross section in the x-z plane, which indicates that the orientation of the dimer lies along the x-direction.

3. Results and Discussion

Before further investigating the structure consisting of a dimer array and a metal film, we first study the hemispherical dimer array only. In order to simulate an infinite unit array

structure, periodic boundary conditions are used in both the x- and y-directions, allowing far-field coupling between dimers [25–27]. When the Rayleigh anomaly (RA) is coupled with localized surface plasmon resonance (LSPR), SLR is formed. Each dimer in the array can be regarded as a dipole, and the static field on each dipole includes the incident field and the sum of the radiated fields of all other dipoles, excluding itself. This causes an increase in the scattering intensity of the array, a narrowing of the spectrum linewidth, and an accompanying strong enhancement of the incoming field [26,28]. Figure 2a illustrates the scattering spectrum of a single hemispherical dimer and the reflectance spectrum of the array structure. We can see that when an array structure is formed, a narrow reflection peak can be found at the wavelength around the array period. Figure 2b,c show the electric field distributions corresponding to the peak wavelengths of the single dimer and dimer array, respectively. The electric field enhancement is mainly concentrated in the vicinity of the hemispheres, with the maximum at the dimer gap. The SLR mode is excited after the formation of the array, and the maximum electric field enhancement factor ($|E|/|E_0|$) between the gap can reach 350, which is about 5 times larger than that of the single dimer. In addition, the Q factor is generally defined as $Q = \lambda_{res}/\Delta\lambda$ (where λ_{res} is the resonance wavelength, and $\Delta\lambda$ is the linewidth of the resonance [29]), and we can note that the Q factor of the array is about 40.

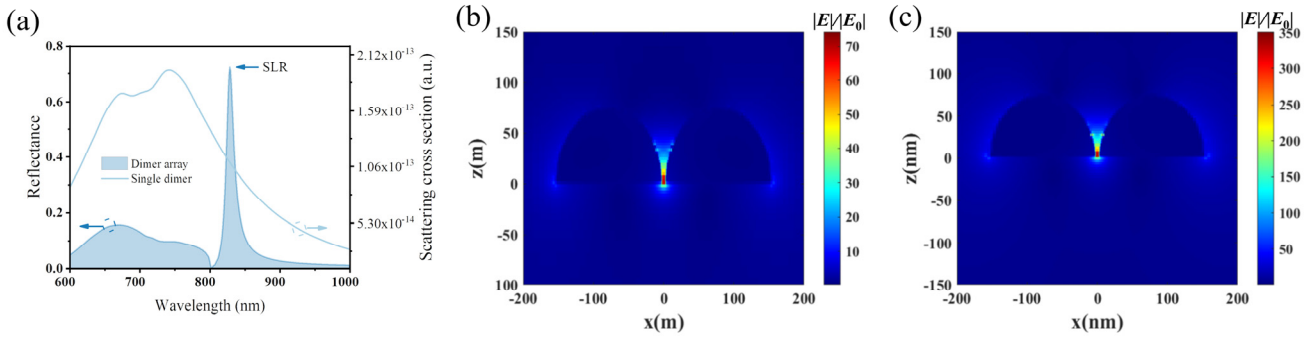

Figure 2. (**a**) Reflection spectrum of hemispherical dimer array and scattering spectra of individual hemispherical dimer. (**b**) Near electric field distribution of single hemispherical dimers. (**c**) Near electric field distribution of hemispherical dimer arrays.

In the next step, we will study structures consisting of dimer arrays and gold films. The dimer array above the gold film can also excite the SLR, and the *RA* can be derived from the following:

$$\lambda_{RAs}^{<i,j>} = n/\sqrt{\frac{i^2}{P_x^2} + \frac{j^2}{P_y^2}} \tag{1}$$

where n is the ambient refractive index around the array, $< i, j >$ is the diffraction order, and P_x and P_y are the lattice period for the array. At the same time, the presence of the array above the gold film allows the *SPP* mode to be excited at normal incidence, which occurs approximately at [30] as follows:

$$\lambda_{SPPs}^{<i,j>} = \frac{P_{x(y)}}{\sqrt{i^2 + j^2}}\sqrt{\frac{\varepsilon_d \varepsilon_m}{\varepsilon_d + \varepsilon_m}} \tag{2}$$

where $\varepsilon_d = n^2$ and ε_m are the dielectric constant of the surrounding medium and the metallic film, respectively. The resonant wavelength of the SPP also varies with the period of the array, which makes SPP mode and SLR mode couple even at normal incidence. It is worth noting that under normal incidence, the diffraction orders degenerate with each other, and the SPP modes and the SLR modes are standing waves due to the interference of oppositely propagating waves [31].

In addition, the resonance of the array can be affected by the formation of a mirror image charge on the gold film. And the mirror image charge is influenced by the distance between the bottom of the array and the top of the gold film (h). When the distance between the array and the gold film is close, the image charge on the film will affect the SLR of the array. When h is large enough, standing waves are generated between the array and the film, leading to the development of FP cavity mode. Therefore, the distance h can be referred to as the cavity length. Figure 3a shows the reflection spectra at different cavity lengths. When the cavity length is between 50 and 150 nm, there are two resonance modes, one of which is located at around 805 nm and does not change much with the cavity length. This can be attributed to the excitation of the SPP mode because lattice spacing is unchanged, and the wavelength of the SPP mode is less influenced. The other resonant mode has a distinct blue shift, which can be attributed to the excitation of the local binding mode of the hybrid structure. The local bonding resonance is governed by the coupling between the dimer and the film, which is significantly influenced by the cavity length. In order to differentiate the two modes, the resonant mode near 805 nm is designated as mode I, and the resonant mode near 825 nm is designated as mode II. When the cavity length exceeds 150 nm, the positions of the two resonance peaks remain basically unchanged. Interestingly, the maximum field enhancement of the two modes is extracted and plotted as a function of cavity length, which is shown in Figure 3b. The field enhancement of mode I almost increases monotonously with the increase in the cavity length, while the field enhancement of mode II drops gradually for the cavity length in the range from 50 nm to 150 nm (reaching the minimum value). Subsequently, the rise of field enhancement of mode II can be seen for the cavity length in the range from 150 nm to 300 nm. Remarkably, field enhancement up to 580 and 480 is attained for mode I and mode II at h = 300 nm, respectively. Up to a 1.7-fold increase in field enhancement is achieved compared to that of SLR mode only (Figure 2c). Such high electric field enhancement is due to the coupling of the SPP mode with the SLR mode, which will be further discussed later.

At this point, the two modes (modes I and II) presented in the reflection spectra are considered the hybrid modes generated by the mode coupling in our array and film system. Interference effect impacting the spectrum significantly, as in a previously reported sub-wavelength structure [32], will play an important role in a large cavity length. Figure 3d,f show the corresponding near-field enhancement distributions and z-component of electric field (E_z) distributions for the two modes at h = 300 nm and 250 nm, respectively. It can be seen that the E_z distribution of λ = 822 nm (h = 250 nm) is very similar to that of λ = 816 nm (h = 300 nm). And at h = 300 nm, the mode profiles of SLR and SPP are preserved for the two hybrid modes. Further enlarging the cavity length h to 350 nm, there is only one resonant mode which is caused by the destructive interferences of FP cavity mode leading to the suppression of the excitation of SLR. This can be proved by the fact that the field enhancement is rather weak at h = 350 nm compared to that of h = 300 nm, as is shown in Figure 3c.

Generally, SPP can be excited by grating structure [33]. In order to clearly manifest the origin of the mode coupling, we turn our dimer array into a one-dimensional grating at h = 300 nm (all other parameters are kept the same), which can be seen in the inset of Figure 4a. A single reflection valley can be seen at the wavelength of 820 nm. By examining the electric field and E_z distribution of the valley wavelength in Figure 4b,c, typical SPP profiles can be found, where maximum field enhancement occurs at the surface of the metallic film. Therefore, the SPP mode is one of the main contributing modes leading to the modal coupling.

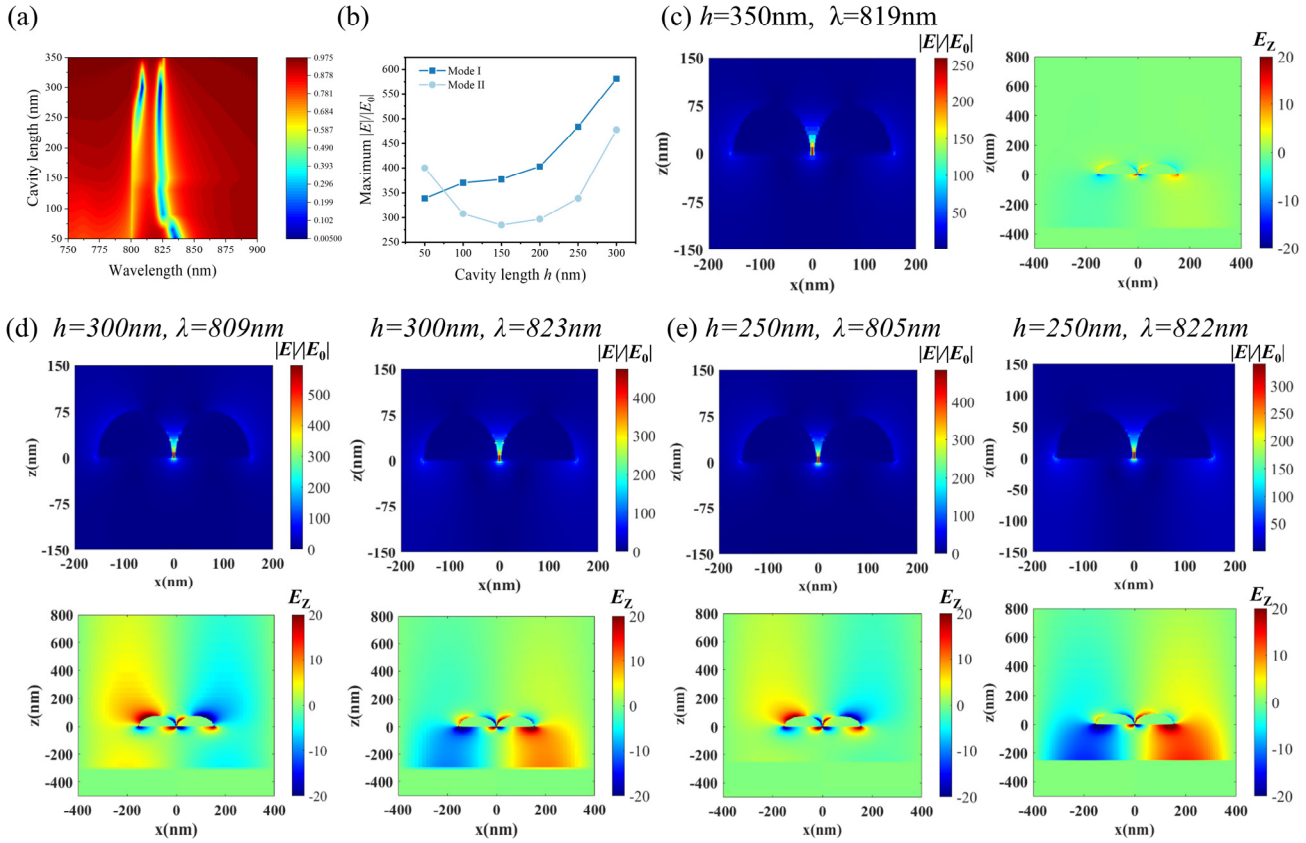

Figure 3. (**a**) Reflection spectra as a function of the cavity length varied from 50 nm to 350 nm. (**b**) Maximum field enhancement $|E|/|E_0|$ with respect to the cavity length (the resonant mode near 800 nm is designated as mode I, and the resonant mode near 825 nm is designated as mode II). Near-filed enhancement distribution and E_z distribution for the resonant wavelength in the *x*-*z* plane when the cavity length (**c**) h = 350 nm, (**d**) h = 300 nm, (**e**) h = 250 nm.

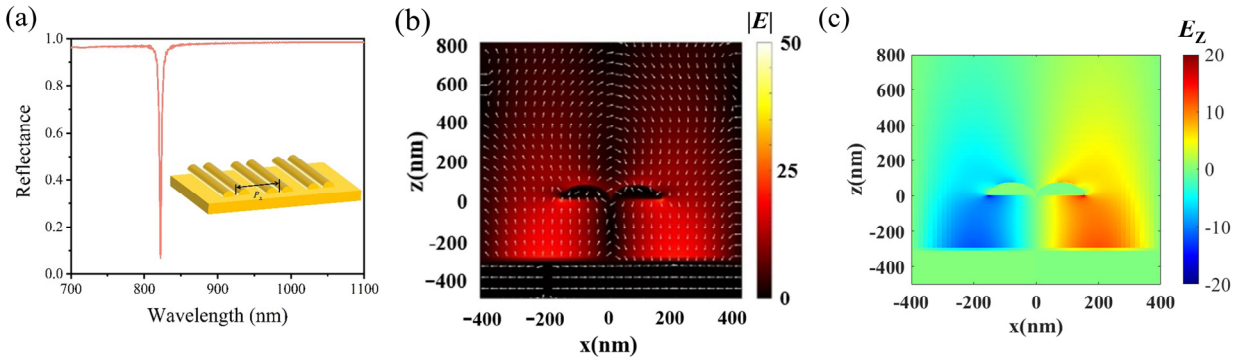

Figure 4. (**a**) Reflection spectrum of a one-dimensional grating with cross section identical to the hemispheric dimer. Inset is the schematic drawing of the one-dimensional grating. h = 300 nm, and all other parameters are kept the same. (**b**) Electric field distribution at the reflection valley wavelength 820 nm. (**c**) E_z distribution at the reflection valley wavelength 820 nm.

Finally, we will show that such a high electric field enhancement results from the coupling between the SLR mode and the SPP mode at h = 300 nm. A coupled oscillator model (COM) is used [34–36],

$$\begin{bmatrix} e_{SLR} + i\gamma_{SLR} & g \\ g & e_{SPP} + i\gamma_{spp} \end{bmatrix} \begin{bmatrix} \beta \\ \eta \end{bmatrix} = e \begin{bmatrix} \beta \\ \eta \end{bmatrix}, \quad (3)$$

where e_{SLR} and e_{SPP} are the resonance energy of the SLR and SPP mode, respectively; γ_{SLR} and γ_{SPP} are the half-widths at half-maximum (HWHM) of the SLR and SPP modes; g is the coupling strength; e is the eigenvalue corresponding to the hybridized modes; and η and β are the eigenvector components (Hopfield coefficients), where the eigenvector components should be satisfied $|\beta|^2+|\eta|^2 = 1$. When the line widths of the SLR and SPP modes are small compared to their energies, the new eigenvalues can be approximated as

$$e_{\pm} = 0.5(e_{SLR} + e_{SPP}) \pm \sqrt{g^2 + \frac{1}{4}\delta^2}. \quad (4)$$

And the Rabi splitting energy ($\hbar\Omega = 2\,g$) can be obtained when $e_{SLR} = e_{SPP}$, where $\delta = e_{SLR} - e_{SPP}$ is the detuning. Considering the excitation condition (normal incident along the z-axis and polarizing along the x-axis), the SLR mode mainly originates from the diffraction coupling along the y-direction. Therefore, P_y determines the SLR mode dominantly. For the SPP mode, the propagation direction is mainly along the x-axis, and the resonant wavelength of SPP is determined by P_x. The above statement can be justified by isolating the two modes, where we turn the material of either the film or dimer array into a perfect electric conductor (PEC). Figure 5 shows the reflection spectra when changing P_x and P_y, respectively. An obvious anti-crossing can be noticed in Figure 5. In addition, the simulated reflection spectra are consistent with the calculated COM results. The coupling strength g related to the Rabi splitting energy is extracted as 12.95 meV (11.05 meV) for altering P_x and P_y, respectively. Although the interaction of the two resonant modes does not enter the region of strong coupling, an increase in the Q factor (~350) for the hybrid modes is obtained compared to that of SLR only in Figure 2.

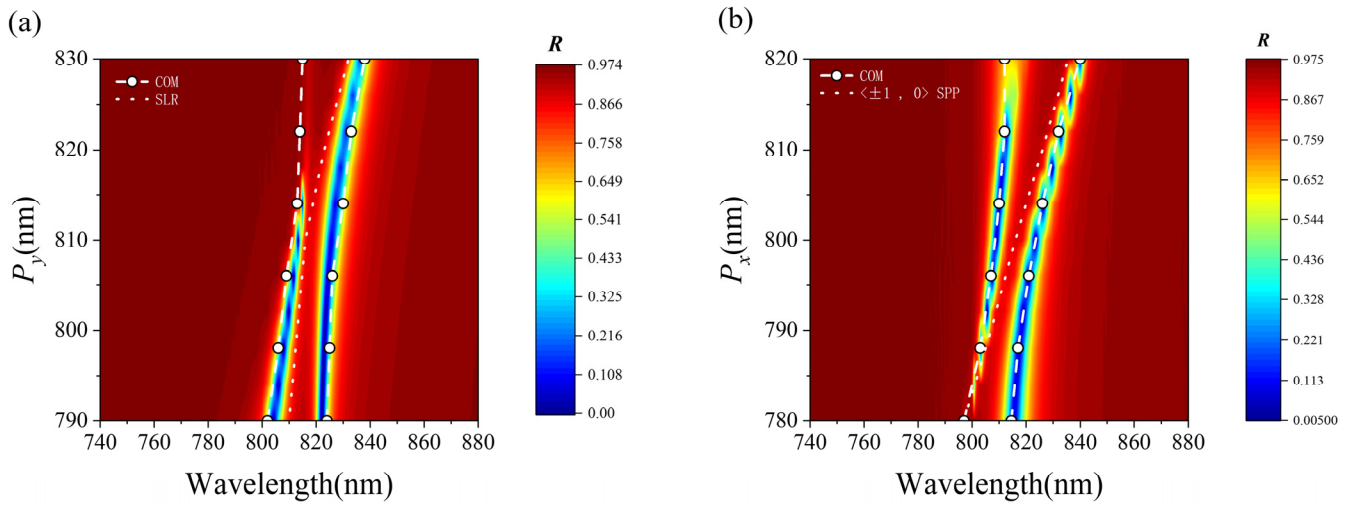

Figure 5. (**a**) Variation in the reflection spectra by adjusting the lattice spacing P_x, P_y = 800 nm. (**b**) Variation in the reflection spectra by adjusting the P_y, P_x = 800 nm. The geometry parameters are kept the same. The white dashed open-circle curves are the calculated results from the coupled oscillator model (COM). The white dotted line in (**a**) is the <±1, 0> SPP mode. The white dotted line in (**b**) is the SLR mode.

4. Conclusions

In conclusion, we investigated the optical responses of hybridized structures consisting of gold films and hemispherical dimer arrays and delved into the role between SLR, SPP, and FP cavity modes at different cavity lengths. The anti-crossings and Rabi splitting are demonstrated in the reflection spectra, which is in agreement with the calculation of the coupled oscillator model. Giant electric field enhancement up to 580 can be achieved due to the coupling of SLR and SPP mode, which shows a 1.7-fold increase compared to that of SLR only. Additionally, the Q factor can also be effectively increased for the hybrid modes. Therefore, we expect that our proposed hybrid structures will provide a versatile

platform for the realization of ultra-sensitive biosensing [37], low-power nonlinear optical devices [38], low-threshold nanolasing [39], etc.

Author Contributions: Conceptualization, J.L. and Z.M.; Methodology, J.L. and Z.M.; Writing—original draft, J.L.; Writing—review & editing, Z.M. and J.Z.; Project administration, J.Z.; Funding acquisition, J.Z. All authors have read and agreed to the published version of the manuscript.

Funding: This work was funded by the Key-Area Research and Development Program of Guangdong Province (2020B090924001) and the Key project of the National Natural Science Foundation of China (62131018).

Institutional Review Board Statement: Not applicable.

Informed Consent Statement: Not applicable.

Data Availability Statement: All Data are available from the authors upon reasonable request.

Conflicts of Interest: The authors declare no conflict of interest.

References

1. Fernández-Domínguez, A.I.; García-Vidal, F.J.; Martín-Moreno, L. Unrelenting plasmons. *Nat. Photonics* **2017**, *11*, 8–10. [CrossRef]
2. Weisman, D.; Carmesin, C.M.; Rozenman, G.G.; Efremov, M.A.; Shemer, L.; Schleich, W.P.; Arie, A. Diffractive Guiding of Waves by a Periodic Array of Slits. *Phys. Rev. Lett.* **2021**, *127*, 014303. [CrossRef]
3. Novotny, L.; Hecht, B. *Principles of Nano-Optics*; Cambridge University Press: Cambridge, UK, 2012.
4. Mandal, P.; Sharma, S. Progress in plasmonic solar cell efficiency improvement: A status review. *Renew. Sustain. Energy Rev.* **2016**, *65*, 537–552. [CrossRef]
5. Alrasheed, S.; Di Fabrizio, E. Effect of Surface Plasmon Coupling to Optical Cavity Modes on the Field Enhancement and Spectral Response of Dimer-Based sensors. *Sci. Rep.* **2017**, *7*, 10524. [CrossRef] [PubMed]
6. Li, H.; Chen, D.-X.; Sun, Y.-L.; Zheng, Y.B.; Tan, L.-L.; Weiss, P.S.; Yang, Y.-W. Viologen-Mediated Assembly of and Sensing with Carboxylatopilla [5]arene-Modified Gold Nanoparticles. *J. Am. Chem. Soc.* **2013**, *135*, 1570–1576. [CrossRef]
7. Zhao, C.; Liu, Y.; Yang, J.; Zhang, J. Single-molecule detection and radiation control in solutions at high concentrations via a heterogeneous optical slot antenna. *Nanoscale* **2014**, *6*, 9103–9109. [CrossRef] [PubMed]
8. Tang, L.; Kocabas, S.E.; Latif, S.; Okyay, A.K.; Ly-Gagnon, D.-S.; Saraswat, K.C.; Miller, D.A.B. Nanometre-scale germanium photodetector enhanced by a near-infrared dipole antenna. *Nat. Photonics* **2008**, *2*, 226–229. [CrossRef]
9. Roxworthy, B.J.; Ko, K.D.; Kumar, A.; Fung, K.H.; Chow, E.K.C.; Liu, G.L.; Fang, N.X.; Toussaint, K.C. Application of Plasmonic Bowtie Nanoantenna Arrays for Optical Trapping, Stacking, and Sorting. *Nano Lett.* **2012**, *12*, 796–801. [CrossRef] [PubMed]
10. Sayed, M.; Yu, J.; Liu, G.; Jaroniec, M. Non-Noble Plasmonic Metal-Based Photocatalysts. *Chem. Rev.* **2022**, *122*, 10484–10537. [CrossRef]
11. Wang, L.; Kafshgari, M.H.; Meunier, M. Optical Properties and Applications of Plasmonic-Metal Nanoparticles. *Adv. Funct. Mater.* **2020**, *30*, 2005400. [CrossRef]
12. Jauffred, L.; Samadi, A.; Klingberg, H.; Bendix, P.M.; Oddershede, L.B. Plasmonic Heating of Nanostructures. *Chem. Rev.* **2019**, *119*, 8087–8130. [CrossRef] [PubMed]
13. Suh, J.Y.; Kim, C.H.; Zhou, W.; Huntington, M.D.; Co, D.T.; Wasielewski, M.R.; Odom, T.W. Plasmonic Bowtie Nanolaser Arrays. *Nano Lett.* **2012**, *12*, 5769–5774. [CrossRef] [PubMed]
14. Crozier, K.B.; Zhu, W.; Wang, D.; Lin, S.; Best, M.D.; Camden, J.P. Plasmonics for Surface Enhanced Raman Scattering: Nanoantennas for Single Molecules. *IEEE J. Sel. Top. Quantum Electron.* **2014**, *20*, 152–162. [CrossRef]
15. Liu, H.; Yang, L.; Liu, J. Three-dimensional SERS hot spots for chemical sensing: Towards developing a practical analyzer. *TrAC Trends Anal. Chem.* **2016**, *80*, 364–372. [CrossRef]
16. Das, G.; Chirumamilla, M.; Toma, A.; Gopalakrishnan, A.; Zaccaria, R.P.; Alabastri, A.; Leoncini, M.; Di Fabrizio, E. Plasmon based biosensor for distinguishing different peptides mutation states. *Sci. Rep.* **2013**, *3*, 1792. [CrossRef]
17. Wang, H.; Levin, C.S.; Halas, N.J. Nanosphere Arrays with Controlled Sub-10-nm Gaps as Surface-Enhanced Raman Spectroscopy Substrates. *J. Am. Chem. Soc.* **2005**, *127*, 14992–14993. [CrossRef]
18. Aizpurua, J.; Bryant, G.W.; Richter, L.J.; García de Abajo, F.J.; Kelley, B.K.; Mallouk, T. Optical properties of coupled metallic nanorods for field-enhanced spectroscopy. *Phys. Rev. B* **2005**, *71*, 235420. [CrossRef]
19. Kessentini, S.; Barchiesi, D.; D'andrea, C.; Toma, A.; Guillot, N.; Di Fabrizio, E.; Fazio, B.; Maragó, O.M.; Gucciardi, P.G.; de la Chapelle, M.L. Gold Dimer Nanoantenna with Slanted Gap for Tunable LSPR and Improved SERS. *J. Phys. Chem. C* **2014**, *118*, 3209–3219. [CrossRef]
20. Hicks, E.M.; Zou, S.; Schatz, G.C.; Spears, K.G.; Van Duyne, R.P.; Gunnarsson, L.; Rindzevicius, T.; Kasemo, B.; Käll, M. Controlling Plasmon Line Shapes through Diffractive Coupling in Linear Arrays of Cylindrical Nanoparticles Fabricated by Electron Beam Lithography. *Nano Lett.* **2005**, *5*, 1065–1070. [CrossRef]

21. Liang, Y.; Koshelev, K.; Zhang, F.; Lin, H.; Lin, S.; Wu, J.; Jia, B.; Kivshar, Y. Bound States in the Continuum in Anisotropic Plasmonic Metasurfaces. *Nano Lett.* **2020**, *20*, 6351–6356. [CrossRef]
22. Wang, Z.; Liang, Y.; Qu, J.; Chen, M.K.; Cui, M.; Cheng, Z.; Zhang, J.; Yao, J.; Chen, S.; Tsai, D.P.; et al. Plasmonic bound states in the continuum for unpolarized weak spatially coherent light. *Photon. Res.* **2023**, *11*, 260–269. [CrossRef]
23. Bai, Y.; Zheng, H.; Zhang, Q.; Yu, Y.; Liu, S.-d. Perfect absorption and phase singularities induced by surface lattice resonances for plasmonic nanoparticle array on a metallic film. *Opt. Express* **2022**, *30*, 45400–45412. [CrossRef] [PubMed]
24. Lide, D.R. *CRC Handbook of Chemistry and Physics*; CRC Press: Boca Raton, FL, USA, 1991.
25. Kravets, V.G.; Schedin, F.; Grigorenko, A.N. Extremely Narrow Plasmon Resonances Based on Diffraction Coupling of Localized Plasmons in Arrays of Metallic Nanoparticles. *Phys. Rev. Lett.* **2008**, *101*, 087403. [CrossRef] [PubMed]
26. Auguié, B.; Barnes, W.L. Collective Resonances in Gold Nanoparticle Arrays. *Phys. Rev. Lett.* **2008**, *101*, 143902. [CrossRef] [PubMed]
27. McLellan, E.; Gunnarsson, L.; Rindzevicius, T.; Kall, M.; Zou, S.; Spears, K.; Schatz, G.; Van Duyne, R. Plasmonic and diffractive coupling in 2D arrays of nanoparticles produced by electron beam lithography. *Mater. Res. Soc. Symp. Proc.* **2007**, *951*. [CrossRef]
28. Kravets, V.G.; Kabashin, A.V.; Barnes, W.L.; Grigorenko, A.N. Plasmonic Surface Lattice Resonances: A Review of Properties and Applications. *Chem. Rev.* **2018**, *118*, 5912–5951. [CrossRef] [PubMed]
29. Barreda, I.; Otaduy, D.; Martín-Rodríguez, R.; Merino, S.; Fernández-Luna, J.L.; González, F.; Moreno, F. Electromagnetic behavior of dielectric objects on metallic periodically nanostructured substrates. *Opt. Express* **2018**, *26*, 11222–11237. [CrossRef] [PubMed]
30. Wang, D.; Guan, J.; Hu, J.; Bourgeois, M.R.; Odom, T.W. Manipulating Light–Matter Interactions in Plasmonic Nanoparticle Lattices. *Acc. Chem. Res.* **2019**, *52*, 2997–3007. [CrossRef] [PubMed]
31. Bahramipanah, M.; Dutta-Gupta, S.; Abasahl, B.; Martin, O.J.F. Cavity-Coupled Plasmonic Device with Enhanced Sensitivity and Figure-of-Merit. *ACS Nano* **2015**, *9*, 7621–7633. [CrossRef]
32. Zheng, D.; Zhang, S.; Deng, Q.; Kang, M.; Nordlander, P.; Xu, H. Manipulating Coherent Plasmon–Exciton Interaction in a Single Silver Nanorod on Monolayer WSe_2. *Nano Lett.* **2017**, *17*, 3809–3814. [CrossRef]
33. Zheng, G.; Xu, L.; Zou, X.; Liu, Y. Excitation of surface phonon polariton modes in gold gratings with silicon carbide substrate and their potential sensing applications. *Appl. Surf. Sci.* **2017**, *396*, 711–716. [CrossRef]
34. As'ham, K.; Al-Ani, I.; Huang, L.; Miroshnichenko, A.E.; Hattori, H.T. Boosting Strong Coupling in a Hybrid WSe_2 Monolayer–Anapole–Plasmon System. *ACS Photonics* **2021**, *8*, 489–496. [CrossRef]
35. Chen, J.; Zhang, T.; Tang, C.; Mao, P.; Liu, Y.; Yu, Y.; Liu, Z. Optical Magnetic Field Enhancement via Coupling Magnetic Plasmons to Optical Cavity Modes. *IEEE Photonics Technol. Lett.* **2016**, *28*, 1529–1532. [CrossRef]
36. Greffet, J.-J.; Carminati, R.; Joulain, K.; Mulet, J.-P.; Mainguy, S.; Chen, Y. Coherent emission of light by thermal sources. *Nature* **2002**, *416*, 61–64. [CrossRef] [PubMed]
37. Li, Z.; Prasad, C.S.; Wang, X.; Zhang, D.; Lach, R.; Naik, G.V. Balancing detectivity and sensitivity of plasmonic sensors with surface lattice resonance. *Nanophotonics* **2023**, *12*, 3721–3727. [CrossRef]
38. Lin, L.; Xue, J.; Xu, H.; Zhao, Q.; Zhang, W.; Zheng, Y.; Wu, L.; Zhou, Z.-K. Integrating lattice and gap plasmonic modes to construct dual-mode metasurfaces for enhancing light–matter interaction. *Sci. China Mater.* **2021**, *64*, 3007–3016. [CrossRef]
39. Zhou, W.; Dridi, M.; Suh, J.Y.; Kim, C.H.; Co, D.T.; Wasielewski, M.R.; Schatz, G.C.; Odom, T.W. Lasing action in strongly coupled plasmonic nanocavity arrays. *Nat. Nanotech* **2013**, *8*, 506–511. [CrossRef]